Influence of Ga vacancies, Mn and O impurities on the ferromagnetic properties of GaN micro- and nanostructures

G. Guzmán, R. Escudero, R. Silva, and M. Herrera

Citation: Journal of Applied Physics **123**, 161578 (2018);
View online: https://doi.org/10.1063/1.5006698
View Table of Contents: http://aip.scitation.org/toc/jap/123/16
Published by the American Institute of Physics

Articles you may be interested in

Acousto–defect interaction in irradiated and non-irradiated silicon n$^+$–p structures
Journal of Applied Physics **123**, 161573 (2018); 10.1063/1.5001123

Multispectral and polarimetric photodetection using a plasmonic metasurface
Journal of Applied Physics **123**, 043107 (2018); 10.1063/1.5011167

Mechanism of yellow luminescence in GaN at room temperature
Journal of Applied Physics **121**, 065104 (2017); 10.1063/1.4975116

Stress management on underlying GaN-based epitaxial films: A new vision for achieving high-performance LEDs on Si substrates
Journal of Applied Physics **122**, 204503 (2017); 10.1063/1.4993985

Role of dislocations and carrier concentration in limiting the electron mobility of InN films grown by plasma assisted molecular beam epitaxy
Journal of Applied Physics **123**, 015701 (2018); 10.1063/1.5008903

Graphene levitation and orientation control using a magnetic field
Journal of Applied Physics **123**, 044302 (2018); 10.1063/1.5005539

Scilight
Sharp, quick summaries illuminating the latest physics research
Sign up for FREE!

JOURNAL OF APPLIED PHYSICS 123, 161578 (2018)

Influence of Ga vacancies, Mn and O impurities on the ferromagnetic properties of GaN micro- and nanostructures

G. Guzmán,[1,2] R. Escudero,[3] R. Silva,[4] and M. Herrera[2,a)]
[1]*Centro de Investigación Científica y de Educación Superior de Ensenada, Posgrado en Física de Materiales, Ensenada, Baja California 22860, Mexico*
[2]*Centro de Nanociencias y Nanotecnología, Universidad Nacional Autónoma de México, Ensenada, 22800 Baja California, Mexico*
[3]*Instituto de Investigaciones en Materiales, Universidad Nacional Autónoma de México, Ciudad de México, Mexico*
[4]*Instituto de Física, B. Universidad Autónoma de Puebla, Puebla 72571, Mexico*

(Received 27 September 2017; accepted 26 December 2017; published online 26 January 2018)

We present a study of the influence of gallium vacancy (V_{Ga}) point defects on the ferromagnetic properties of GaN:Mn and GaN:Mn,O micro- and nanostructures. Results demonstrate that the generation of these point defects enhances the ferromagnetic signal of GaN:Mn microstructures, while incorporation of oxygen as an impurity inhibits this property. XPS measurements revealed that Mn impurities in ferromagnetic GaN:Mn samples mainly exhibit a valence state of 2+. Cathodoluminescence (CL) spectra from Mn-doped GaN samples displayed emissions centered at about 1.97 eV, attributed to transitions between the $^4T_1$-$6A_1$ states of the Mn^{2+} d orbitals, and emissions centered at 2.45 and 2.9 eV, associated with the presence of V_{Ga}. CL measurements also revealed a blue shift of the GaN band-edge emission generated by the expansion of the *wurtzite* lattice due to Mn incorporation, which was confirmed by XRD measurements. These latter measurements also revealed an amorphization of GaN:Mn due to the incorporation of oxygen as impurities. The GaN:Mn samples were synthesized by thermal evaporation of GaN and $MnCO_3$ powders onto $Ni_{0.8}Cr_{0.2}$/Si(100) in a horizontal furnace operated at low vacuum. The residual air inside the system was used as a source of oxygen during the synthesis of Mn and O co-doped GaN nanostructures. Mn and O impurities were incorporated into the nanostructures at different concentrations by varying the growth temperature. Energy Dispersive Spectroscopy, XRD, and XPS measurements confirmed that the obtained samples predominantly consisted of GaN. *Published by AIP Publishing.*
https://doi.org/10.1063/1.5006698

I. INTRODUCTION

Gallium oxide is a wide bandgap semiconductor (3.4 eV at room temperature) used to fabricate efficient laser and light-emitting diodes.[1–4] In recent years, this material has also received attention in spintronic applications. Since Dietl *et al.* proposed that GaN and ZnO doped with magnetic impurities at low concentration can exhibit ferromagnetism at room temperature,[5] several authors have reported evidence of this property using Mn as a magnetic impurity in GaN.[6–9] However, the origin of ferromagnetism in GaN and other dilute magnetic semiconductors (DMS) is not clear because conventional super-exchange or double-exchange interactions do not adequately explain the long-range magnetic order observed for magnetic impurities at low concentrations.[10–13] Some reports have proposed that ferromagnetism in DMS is generated by exchange interactions mediated by the point-defects present in semiconductors; consequently, much effort has been devoted to achieving precise control in point-defect generation during the synthesis of GaN:Mn.[14–17] On the other hand, adequate control of the valence configuration of magnetic impurity ions in GaN is essential, particularly because the incorporation of Mn^{2+} ions into GaN atoms, as acceptor impurities, has been reported to generate holes that act mediating the generation of ferromagnetism.[13] Therefore, as the generation of ferromagnetism by exchange interactions mediated by point defects and impurities is very probable in DMS, their identification in GaN produced by doping it with Mn can certainly help in the study of these spin interactions. In this work, we used the Cathodoluminescence (CL) technique to study the defect structure in GaN micro- and nanostructures generated by the incorporation of Mn and O at different concentrations. Besides, we used a SQUID system to measure the ferromagnetic response of GaN:Mn samples. Results suggest that the incorporation of Mn impurities generates type V_{Ga} point defects, which enhance the ferromagnetic signal of GaN:Mn microstructures, while the incorporation of oxygen inhibits this property. In addition, XPS measurements revealed that Mn impurities in GaN mainly exhibited a valence state of 2+.

II. EXPERIMENTAL

Undoped GaN and Mn-doped GaN micro- and nanorods were synthesized by thermal evaporation of GaN powder (Alfa Aesar, 99.9%) or GaN mixed with $MnCO_3$ powders (Alfa Aesar, 99.9%) onto $Ni_{0.8}Cr_{0.2}$/Si(100) substrates in a homemade horizontal quartz tube furnace operated at 900

[a)]Author to whom correspondence should be addressed: zaldivar@cnyn.unam.mx. Tel.: (646) 175-0650.

mTorr. The non-magnetic nichrome $Ni_{0.8}Cr_{0.2}$ buffer layer deposited by thermal evaporation onto Si(100) allowed optimal adherence of the GaN structures with the substrates. As shown in Table I, four samples were synthesized at temperatures and growth times in accordance with previous studies,[18,19] using NH_3 (Infra 99.9%) as carrier gas at flows between 12 and 16 sccm. The powder mix was placed in an alumina boat at the center of the furnace, evaporated at 1200 °C, and diffused upstream of the ammonia flow toward four aligned NiCr/Si(100) substrates along the quartz tube. A thermocouple measured the growth temperature, recording values of about 900 °C (sample 2), 850 °C (sample 3), 800 °C (sample 4), and 750 °C (sample 5). The selected growth temperature was within the interval of the previously determined optimal temperatures to obtain the desired morphology and size of the structures in our furnace. In addition, we had control of the atomic percentage of the impurity (O or/and Mn). In previous work, we found that at temperatures from 850 to 600 °C, O is incorporated as an impurity at atomic percentages that range from 5% to 18%. The higher the growth temperature, the lower the atomic percentage of O, and at growth temperatures lower than 600 °C, oxides like Ga_2O_3 tended to form.[20] Incorporation of oxygen originating from the residual air in the furnace was found only in samples 4 and 5 (Table I). An undoped GaN sample (sample 1) was also synthesized onto a NiCr/Si(100) substrate, at 950 °C, to compare its properties with the Mn-doped samples.

The crystal structure was characterized with a Philips X'pert X-ray diffractometer with a CuKα ($\lambda = 0.154$ nm) line excitation source with a tension of 45 kV and current of 40 mA. Detector condition slits were S1 (divergence slit) $\frac{1}{2}$Å and S2 (anti-scatter slit) 1 Å that correspond to a resolution of 0.08° (Degree) equivalent to 0.008 Å in accordance with that reported by the User Manual Philips X'pert X-ray Diffractometer. The relative atomic composition of the samples was characterized by Energy Dispersive Spectroscopy (EDS) using an Oxford X-Max analyzer equipped with silicon drift detector X-Max and INCA X-Stream 2 and MICS 2 Software (Oxford Instruments). The uncertainty in the atomic percentage of each element corresponded to the standard deviation (sigma) of the calculation done by the INCA software, operated with a standard-based sequence. The energy of the EDS electron beam was 15 keV with a current of 3.1×10^{-8} A. The measurements in samples S1, S3, and S5 were taken at magnification of 3000×, S2 in an area of approximately 1 μm^2 due to the size of sample and the microstructures, and the measurement in sample S4 was taken at a magnification of 8000× (see supplementary material). Correct calibration of the EDS system was confirmed by measuring the relative concentration of a GaN epitaxial film (MTI Corp., Stock No. GaNTsi50D05C1-N), which yielded values of Ga and N of 50.2 (±0.7) and 49.7 (±0.4) at. %, respectively. For Transmission Electron Microscopy (TEM) and Selected Area Electron Diffraction (SAED) measurements, a JEOL JEM 2100 which was operated at 200 keV and equipped with an EDS X-Max Oxford-Instrument was used to obtain high resolution images of the nanowires of samples S4 and S5 and study the defects in the atomic layers induced by the incorporation of Mn and O in the GaN lattice. SAED in TEM was used to confirm and quantify the presence of Mn an O as impurities in the nanowires. A SPECS system equipped with a PHOIBOS WAL analyzer using an Al anode was used to measure the X-ray photoelectron (XPS) signals emitted from the samples. High-resolved spectra for each element present in the samples were obtained after 300 accumulative measurements. The obtained XPS spectra were calibrated using the C (1s) signal (284.6 eV) as reference. Sample morphology was studied using a JEOL FIB-4500 SEM and a field emission JEOL JSM-7800F equipped with a STEM system. A Mono-CL4 Gatan system adapted to the JEOL FIB-4500 SEM system measured the cathodoluminescence (CL) signal from samples at room temperature and in the UV-visible spectral range. A SQUID (MPMS-5S) Quantum Design magnetometer (from IIM-UNAM, Mexico City) with a resolution of 1×10^{14} T operated in Reciprocating Sample Option (RSO) mode was used to detect the magnetic response of the samples by applying a magnetic field from ±1 T parallel to the surface of the samples at 100 K.

III. RESULTS AND DISCUSSION

Table I shows that all synthesized samples contained a higher concentration of nitrogen than gallium, apparently due to the N-rich conditions generated by placing the substrates at the upstream of the NH_3 flow in the furnace. This gallium deficiency could promote the formation of gallium vacancies (V_{Ga}), since these point defects exhibit the lower formation energy for GaN grown under N-rich conditions.[21] Table I also shows, for samples 2 and 3, that a lower amount of manganese was incorporated into GaN as the growth temperature increased. EDS measurements from samples 4 and 5 similarly revealed that, by lowering the growth temperature, the Mn and O concentrations increased. EDS measurements did not reveal Ni or Cr signals.

As stated in the Experimental section, the conditions to obtain the atomic percentage were not the same for all samples. Nevertheless, our purpose was to obtain a representative quantification of the elements contained in each sample. For this, several EDS measurements were taken for each sample

TABLE I. Growth conditions and elemental composition of GaN samples measured by EDS in SEM.

Sample No.	Growth Temp. (°C)	Ga (at. %) ± 0.7	N (at. %) ± 0.4	Mn (at. %) ± 0.03	O (at. %) ± 0.3	NH_3flow (sccm)	Time (h)
1	950	45	55	…	…	12.15	4.6
2	900	43.1	52.7	4.2	…	16.05	5
3	850	37.2	53.9	8.9	…	12	4.6
4	800	39.7	47.8	2.6	9.9	12.3	3.5
5	750	36.2	40.1	5.7	18.0	12	4.6

from different areas, and the representative percentage of all measures is presented in this paper. For samples S4 and S5, SAED measurements were made to confirm the presence of Mn and O impurities in the nanowires, not only their detection in the bulk. The most relevant result revealed by these measurements is that the atomic percentage of Mn and O as impurities in the nanowires is in fact the same as in the bulk and that their distribution along the nanowires is homogeneous. These results, however, are not presented in this paper.

Figure 1 shows normalized XRD patterns of the samples with diffracting peaks that correspond with the *wurtzite*-type crystal structure of the GaN. Sample 1 shows similar relative intensities for the main (100), (002), and (101) diffraction peaks, with Bragg angles that correspond to lattice parameter values of $a = b = 3.18$ Å and $c = 5.18$ Å, calculated by using *Carine Crystallography* software. Samples 2–5 show a gradual shift of the (100) and (101) diffraction peaks –relative to the (002) peak, because its measured value was the same for all samples to lower Bragg angles as Mn concentration increased within them, revealing a gradual expansion of the lattice parameters a and b. For samples 2 and 3, we calculated that these parameters increased by 0.01 and 0.027 Å, respectively, with respect to the reference values measured for sample 1. This result demonstrates that Mn incorporates as substitutional impurity (Mn_{Ga}) in the *wurtzite* basal plane (001), defined by the $\boldsymbol{a}$ and $\boldsymbol{b}$ unit cell vectors, generating its expansion, apparently because Mn ions have higher ionic radius than Ga ions. We propose that Mn^{2+} ions substitute Ga^{3+} ions because 2+ is the most stable oxidation state of Mn and because Mn^{2+} has a larger ionic radius than the ionic radius of Ga^{3+} (67 and 62 pm, respectively). Figure 1 also shows that sample 2 exhibited higher relative intensity of the (002) diffraction peak than other samples, which corresponds to the formation of hexagonal prismatic structures, as revealed by SEM measurements (Fig. 4). Sample 3, in contrast, shows a low relative intensity of the (002) peak and high relative intensities of the (100) and (101) diffraction peaks, suggesting alternated growth of the [100] and [001] directions of the *wurtzite* structure. XRD patterns from samples 4 and 5 show diffraction peaks with lower intensities and

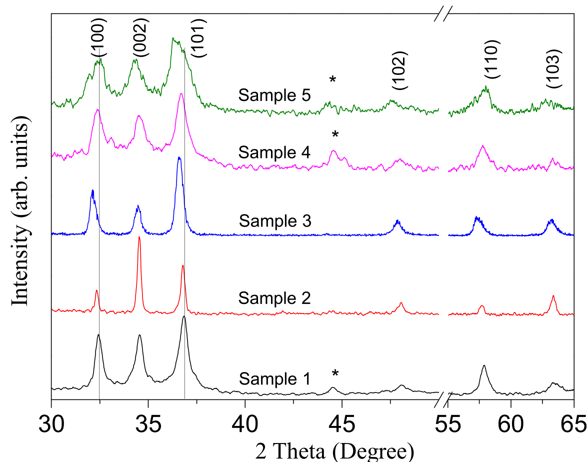

FIG. 1. XRD patterns of samples (1-black, 2-red, 3-blue, 4-magenta, and 5-green lines, respectively) show the hexagonal crystalline structure of GaN. *Peak associated with the substrate. Reference JCPDS 76-0703.

wider than other samples, revealing that oxygen incorporation reduces the GaN:Mn crystalline quality. XRD measurements do not show diffraction peaks corresponding to β-Ga_2O_3 monoclinic, Ga_3O_3N spinel-type, GaNO sphalerite-type, or manganese oxide (MnO) as residual phases.

The chemical state of the elements present on the surface of samples was determined by XPS measurements. Figure 2(a) shows the XPS spectra of the N 1s signal obtained from GaN sample 1 centered at about 397 eV, which correspond to the N-Ga bonding. Similarly, all samples revealed the Ga $2p_{3/2}$ and Ga $2p_{1/2}$ signals centered about at 1117.4 and 1144.2 eV, respectively, matching with those reported for epitaxial GaN.[22] Figure 2(c) shows the O 1s signal from the samples centered at 531.5 eV that corresponds to the C=O bond of the adsorbed residual atmospheric gases.[23] This XPS signal also shows one shoulder at about 529.8 eV for samples 3–5, which could correspond to the binding energy of Ga-O or Mn-O bonds.[24] Nevertheless, EDS in SEM did not detect an O signal in sample 3. Figure 2(d) shows the Mn 2p signal as two peaks produced by its splitting due to spin-orbit coupling effects. These Mn $2p_{1/2}$ and $2p_{3/2}$ signals exhibited binding energies of 653 and 641 eV, respectively, matching with the reported values for the Mn-N bond.[25,26] Figure 2(d) also shows a shoulder at about 646 eV that we assign to the well-known satellite signal observed for Mn^{2+} ions.[25]

Figure 3 shows the deconvoluted $2p_{3/2}$ signal peak calculated for sample 3 with two Gaussian curves centered at 641 and 642 eV, which correspond to the Mn^{2+} and Mn^{3+} signals, respectively.[27,28] This result reveals that the Mn 2p signal detected at the surface of the sample is produced mainly by divalent Mn ions, in agreement with other reports. Hwang *et al.* previously reported for $Ga_{1-x}Mn_xN$ thin films that Mn ions incorporate into the tetrahedral sites of the wurtzite structure as substitutional impurities and that their valence is divalent.[28] Other authors, besides, have found that the valence of the Mn ions depends on the growth temperature of their host material during synthesis. Mn^{+3} incorporates at growth temperatures above 980 °C, both Mn^{+3} and Mn^{+2} at temperatures between 980 and 900 °C, and Mn^{+2} at temperatures below 900 °C.[29,30] Since growth temperature of most of the samples was lower than 900 °C, a high concentration of Mn^{2+} was expected in them, correlating with XPS results.

SEM images from sample 1 show formation of elongated microplates of several microns in length, 1 μm in width, and about 500 nm in thickness [Fig. 4(a)]. These structures showed triangular ends apparently due to the growth of GaN along the $[11\bar{2}0]$ directions. Figures 4(b) and 4(c) show that Mn-doped GaN samples grew forming hexagonal prismatic microstructures. Sample 2 revealed the formation of embedded prisms of about 7 μm in length and radius between 1 and 2.5 μm, while sample 3 exhibited the formation of both regular hexagonal prisms [red rectangles in Fig. 4(c)] and prismatic structures elongated along the $[11\bar{2}0]$ directions [white rectangle inset in Fig. 4(c)]. SEM images of the Mn and O co-doped samples show the formation of GaN nanowires of several microns in length and diameters smaller than 500 nm, as shown Figs. 4(d) and 4(e) for samples 4 and 5, respectively. Sample 5 also shows the

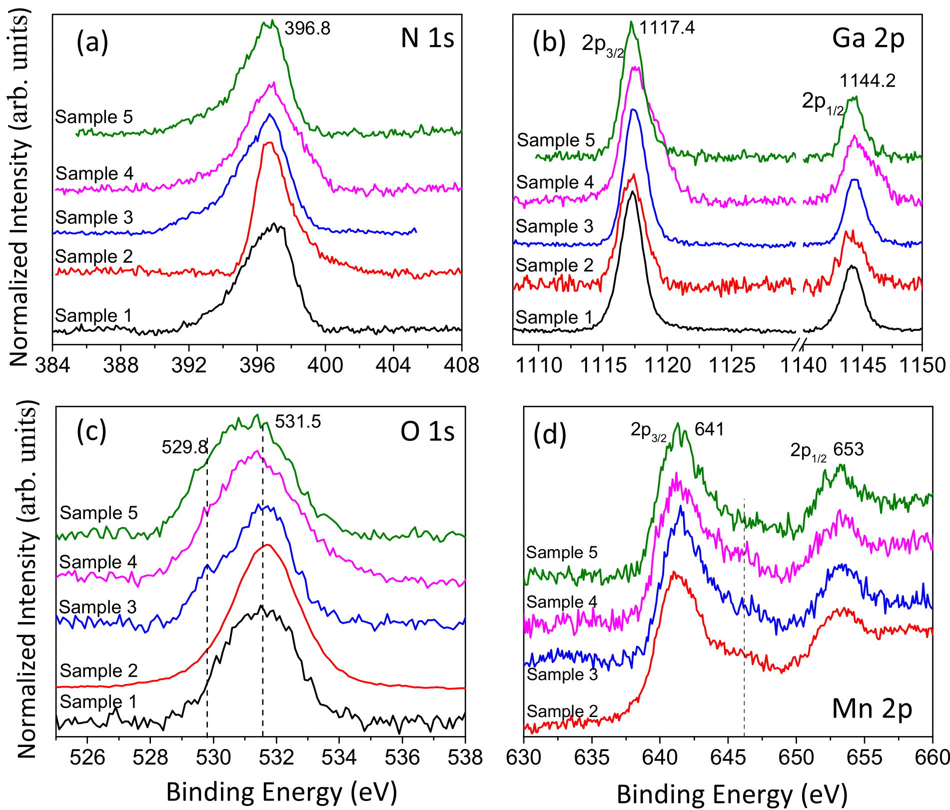

FIG. 2. High resolution XPS spectra of the elements (a) N (1s), (b) Ga (2p), (c) O (1s), and (d) Mn (2p) present on the surface of the samples (1-black, 2-red, 3-blue, 4-magenta, and 5-green lines, respectively). Graphs (c) and (d) revealed that there is no Mn-O bond. The binding energy of the Mn doublet $2p_{3/2}$ and $2p_{1/2}$ and the presence of a satellite component indicate that the Mn^{+2} ion is occupying Ga sites. Binding energy values of the O peak 1s suggest the presence of oxygen on surface due to atmospheric adsorption.

formation of bent microwires of about 1 μm in diameter and several microns in length, exhibiting a rough surface, possibly generated by the stacking of circular plates.

Figure 5(a) shows a typical TEM image of a nanowire of sample 4, which displays the characteristic dark fringes transverse to its growth direction. We had previously identified these line defects as edge dislocations[31] generated by atomic stacking faults (planar defects[32]) that promote the incorporation of oxygen into the GaN lattice at high concentrations.[19] HRTEM images obtained near the end of one of these nanowires show atomic planes spaced by approximately 5 Å corresponding to the wurtzite (0001) planes [inset in Fig. 5(b)]. Figure 5(c) shows a region of the nanowire with atomic faults in the stacking sequence of the basal planes (0001) (dashed orange lines that are misaligned with the blue lines). Similar stacking faults we had previously observed in oxygen-doped GaN nanowires and attributed their origin to the formation of extended defects such as dislocations or twinning defects.[19] TEM images from nanowires of the sample 5 show similar stacking fault defects as observed in sample 4.

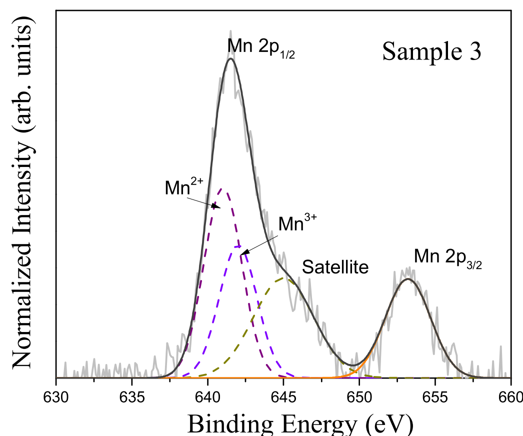

FIG. 3. A deconvolution of peak Mn $2p_{3/2}$ of sample 3 suggests a major presence of Mn^{2+} and a minor possible presence of the Mn^{+3} ion, but the clear presence of the component associated with the satellite confirms the divalent state of the Mn ion.

Figure 6(a) shows the normalized CL spectra obtained from samples 1 and 2, revealing emissions centered at 3.19 and 3.35 eV that correspond to the GaN band-edge signals, respectively. The blue shift of this emission observed for sample 2 is attributed to the expansion of the *wurtzite* lattice due to Mn incorporation, such as has been previously reported for Mn-doped GaN epitaxial films.[33] Figure 6(a) also shows that sample 1 reveals a broad and weak emission in the range 1.7–2.8 eV [arrows in Fig. 6(a)], composed by two emissions centered at about 2.0 and 2.5 eV as shown in the inset in Fig. 6(a). The first band corresponds to the well-known yellow emission of GaN, the origin of which is still subject of controversy; however, it has been associated with native point-defects of the nitrogen vacancies type (V_N) by several authors.[18,34,35] The second band, centered at around 2.5 eV, could correspond to the green emission of GaN previously reported by Reshchikov and Morkoç in undoped GaN films, therein assigned to gallium vacancies (V_{Ga}).[36] Figure 6(b) shows the CL spectrum for sample 3, which reveals a broad emission covering the complete visible electromagnetic range with a maximum at 1.97 eV. A deconvolution of this spectrum is also shown in Fig. 6(b), calculated by using four Gaussian curves centered at 1.97, 2.45, 2.9, and 3.3 eV, with FWHM of 0.4 eV for the first three components and 0.2 eV for the last. The predominant component of

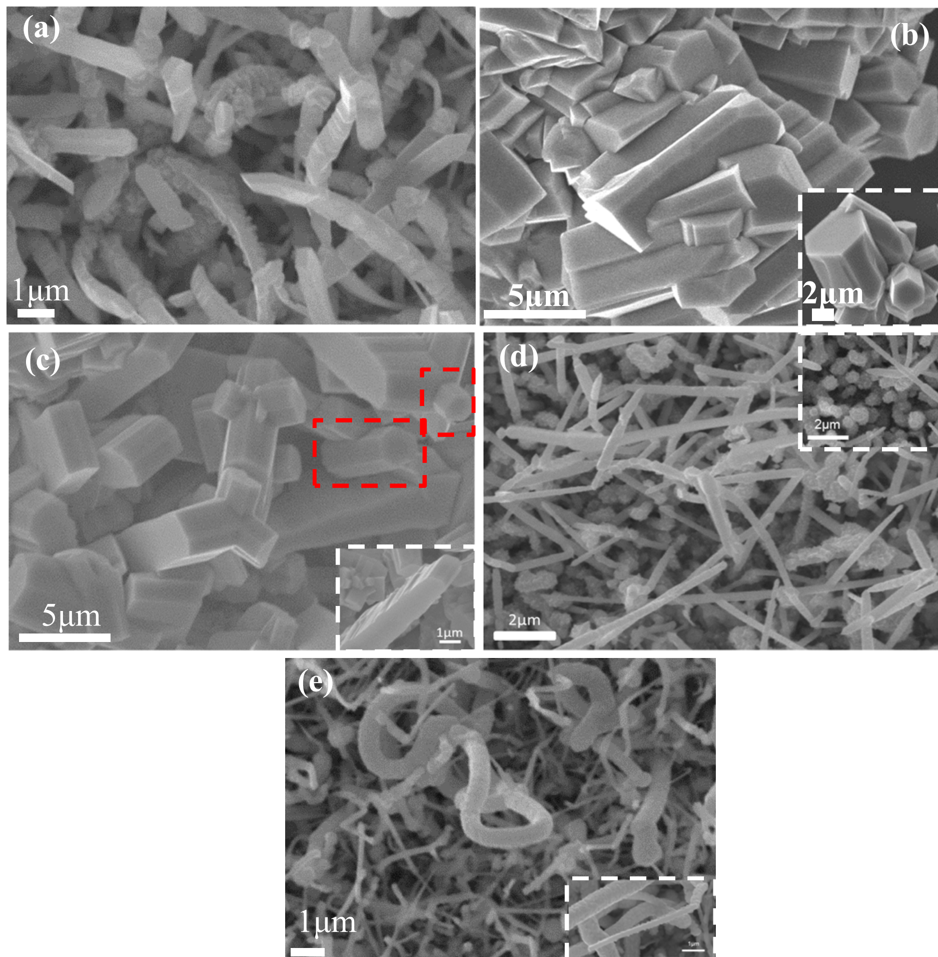

FIG. 4. Secondary electron images of micro-nanostructures of: pure GaN (a) sample 1; Mn-doped GaN (b) sample 2 and (c) sample 3; GaN codoped with Mn and O (d) sample 4 and (e) sample 5. Inset in (b) shows hexagonal micro-rods present in sample 2. In sample 3, red rectangles mark hexagonal micro-rods, and inset in (c) shows a wire grown in the $[11\bar{2}0]$ direction. Inset in (d) shows nanocrystals below the nanowires in sample 4. Inset in (e) shows a granular surface of the nanowires of sample 5.

1.97 eV could corresponds to the emission of 2.03 eV reported by Joshi *et al.* for Mn-doped GaN monocrystals assigning an origin to transitions between the $4T_1$-$6A_1$ states of the d orbitals of Mn^{2+}.[37] However, Graf *et al.* previously reported that Mn doping of GaN epitaxial films generates $Mn^{3+/2+}$ acceptor levels at 1.8 eV above the valence band,

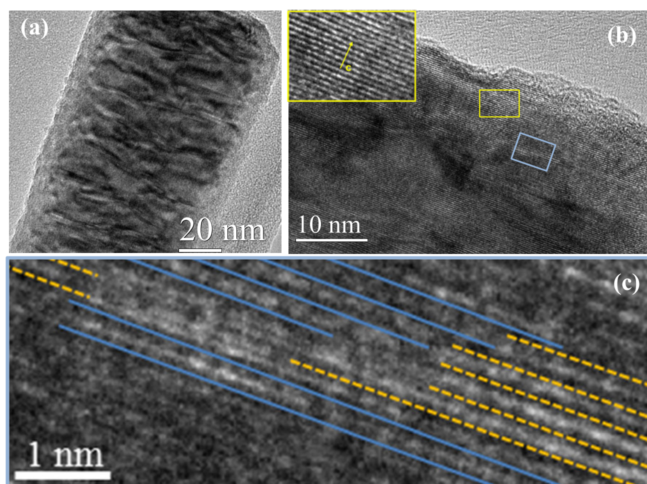

FIG. 5. (a) TEM image of a typical nanowire from sample 4, showing line defects. (b) HRTEM image from the tip of the nanowire; yellow inset indicates wire growth in the c-direction. (c) Zoom of the blue rectangle from (b), showing dislocations of the atomic lines; dashed orange atomic lines are misaligned with the blue atomic lines.

which produces an absorption band at this same energy.[38] Radiative electronic transitions between this acceptor level are not identified in Fig. 6(b) although we do not discard their presence. The band of 2.45 eV, as commented before, was attributed to the presence of V_{Ga} in GaN.[36] The blue band centered at 2.9 eV was studied by Xu *et al.* in epitaxial GaN films, and its origin was ascribed to metastable defects type V_{Ga}.[39] Other authors have attributed this blue emission to electronic transitions from either a shallow donor or conduction band to deep acceptors located at 0.4 eV above the valence band.[40]

Calculations using the local-density functional method reported by Elsner *et al.* for V_{Ga} trapped in threading dislocations in GaN exhibit different energy level values as a function of the atomic position of vacancies close to a dislocation.[41] At the nearest atomic position in the stress field close to the dislocation core, they reported a value of 0.4 eV above the valence band for the energy transition level 3-/2-. In a previous CL study, we reported that the 2.9 eV emission of GaN is generated by decorating dislocations caused by point defects.[42] We propose that the blue band of 2.9 eV corresponds to electronic transitions between acceptor levels produced by V_{Ga} trapped in threading dislocations. Gallium vacancy generation in sample 3 apparently obeys to the excessive distortion of the GaN lattice due to the high Mn incorporation, as shown Fig. 1. The band of 3.3 eV in Fig. 6(b) corresponds to the GaN band edge emission. The CL spectrum from sample 4, shown in Fig. 6(c), also exhibited a

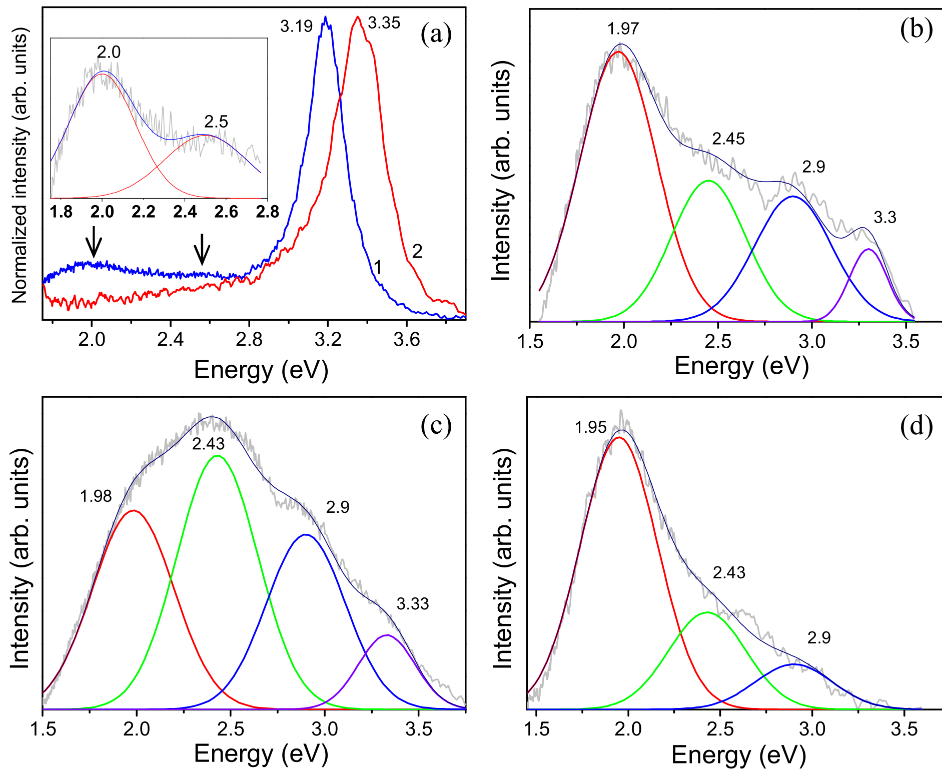

FIG. 6. CL spectra of samples (a) 1 and 2; a deconvoluted CL spectrum of the defect range in sample 1 is shown in the inset, where two main components centered at 2 and 2.5 eV are visible that correspond to a typical native defect in GaN. Deconvoluted CL spectra of samples (b) 3, (c) 4, and (d) 5 are presented. The component centered at 1.98 eV is associated with the presence of Mn in the lattice of GaN. Components centered at 2.43 and 2.9 eV are associated with native defects such as V_{Ga} generated in GaN by the presence of Mn and an N-rich atmosphere during synthesis. In samples 2, 3, and 4, the presence of the bandgap at high energy corresponds to the shift to high energy due to the incorporation of Mn into the crystalline structure of GaN.

broad emission with components at 1.98, 2.43, 2.9, and 3.33 eV, which correspond to those observed in sample 3 [Fig. 6(b)]. Since the 2.43 eV emission dominated the CL spectrum, a high concentration of V_{Ga} point defects is expected in this sample. Sample 5 revealed a CL spectrum similar to that observed for sample 3 although with lower intensity for the emissions related to V_{Ga} and the absence of the GaN band edge emission due to the lack of crystallinity of the sample, as shown in Fig. 1. For spatial distribution of the defects attributed to the blue, green, and red emission, CL images were taken and are shown in Fig. 7 for sample 3.

Figure 7 shows secondary and the corresponding monochromatic CL images of sample 3, obtained by using band-pass filters with center wavelengths of 620 nm [2.0 eV, Fig. 7(b)], 470 nm [2.6 eV, Fig. 7(c)], and 400 nm [3.1 eV, Fig. 7(d)]. The red emission shows an almost homogeneous distribution at the microstructures, suggesting uniform incorporation of Mn^{2+} into GaN. In contrast, the green and blue bands show high CL intensity at the edges, revealing an inhomogeneous distribution of V_{Ga} in sample 3.

For magnetic characterization of samples, we first studied the magnetic response of the NiCr/Si substrates to discriminate in the magnetization generated by the Mn-doped GaN. Figure 8(a) shows a typical magnetization vs. magnetic field (M-H) curve obtained from a NiCr/Si substrate, revealing a clear diamagnetic behavior under applied magnetic fields greater than $\pm$0.25 T. Besides, at magnetic intensities lower than $\pm$0.2 T, the substrate exhibited a residual ferromagnetic signal, whose origin is not clear because neither the Si(100) nor the NiCr alloy has magnetic response, according to the manufacturer's data.

On the other hand, the H-M curve from sample 1 revealed a similar magnetic response as the NiCr/Si substrate, shown in Fig. 8(b), although with a better defined ferromagnetic signal. Weak ferromagnetism in undoped GaN has been reported by other authors attributing its origin to the polarization of unpaired 2p electrons of N surrounding Ga vacancies.[29] However, since the NiCr/Si substrates exhibited residual ferromagnetism, a clear ferromagnetic signal associated only with pure GaN cannot be confirmed (sample 1). In contrast, M-H curves from Mn-doped samples 2 and 3 revealed a clear ferromagnetic signal overlaying the diamagnetic response of the substrate [Figs. 9(a) and 9(b)]. The coercivity and the saturation magnetization values for sample 2 were 0.030 T and 8.1×10^{-5} emu, while for sample 3 the values were 0.048 T and 6.5×10^{-5} emu, respectively. Although sample 3 does not seem to have a saturation point, this can be due to the strong paramagnetic response of GaN at high values of the applied magnetic fields, above/below $\pm$0.25 T.

The increase in coercivity with the Mn concentration in samples S2 and S3 demonstrates that this impurity promotes ferromagnetism in GaN as was expected. Previously, Hori *et al.* reported that Mn impurities in GaN films at concentrations between 3% and 5% increase the Curie temperature above room temperature. These authors proposed a double-exchange interaction between the t_{2g} anti-bonding orbitals of the Mn ions as the mechanism of ferromagnetism generation.[43] On the other hand, the origin of ferromagnetism must not necessarily be assigned only to changes in the concentration of magnetic impurities because, as other authors have been commented, point defects in the semiconductor host can mediate the exchange interactions of the magnetic ions.[15,17] Correlating with the presence of defects shown in the CL spectra in Fig. 6, the increase of Mn concentration in GaN from 4.2 at. % (sample 2) to 8.9 at. % (sample 3) causes V_{Ga} point-defects that could participate in the generation of

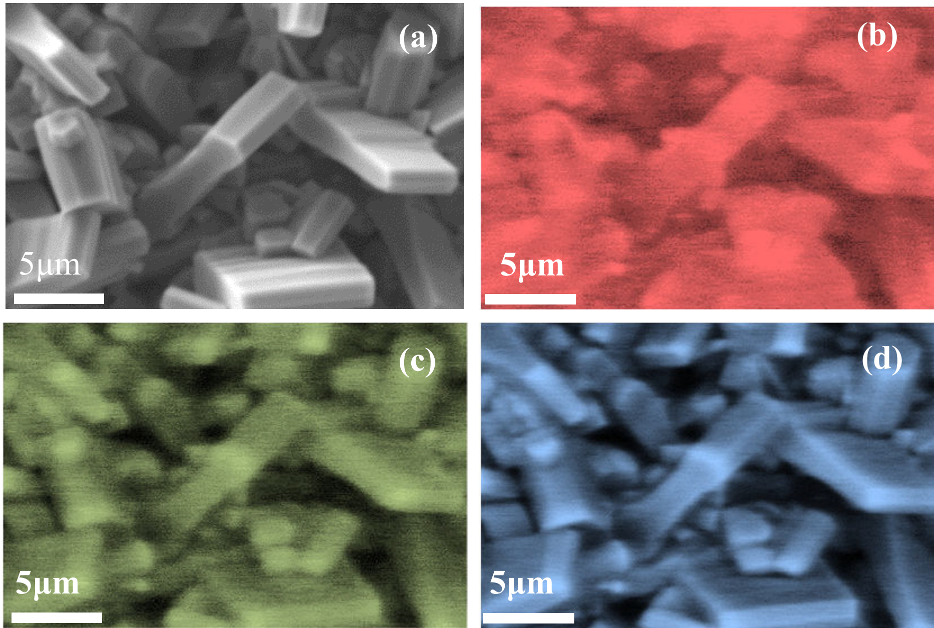

FIG. 7. (a) Secondary and (b)–(d) monochromatic CL images from sample 3. (c) and (d) show a similar distribution of the defects associated with blue (2.9 eV) and green (2.4 eV) emission components. Meanwhile (b), which corresponds to the emission centered at 1.9 eV, shows a different distribution for the component associated with the presence of Mn.

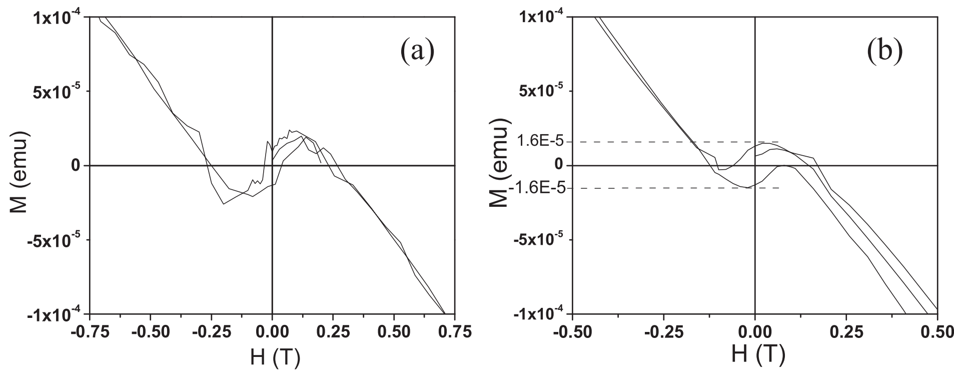

FIG. 8. M-H raw curves at 100 K of the (a) NiCr/Si substrate and (b) sample 1 (GaN) showing a strong diamagnetic response associated with the substrate.

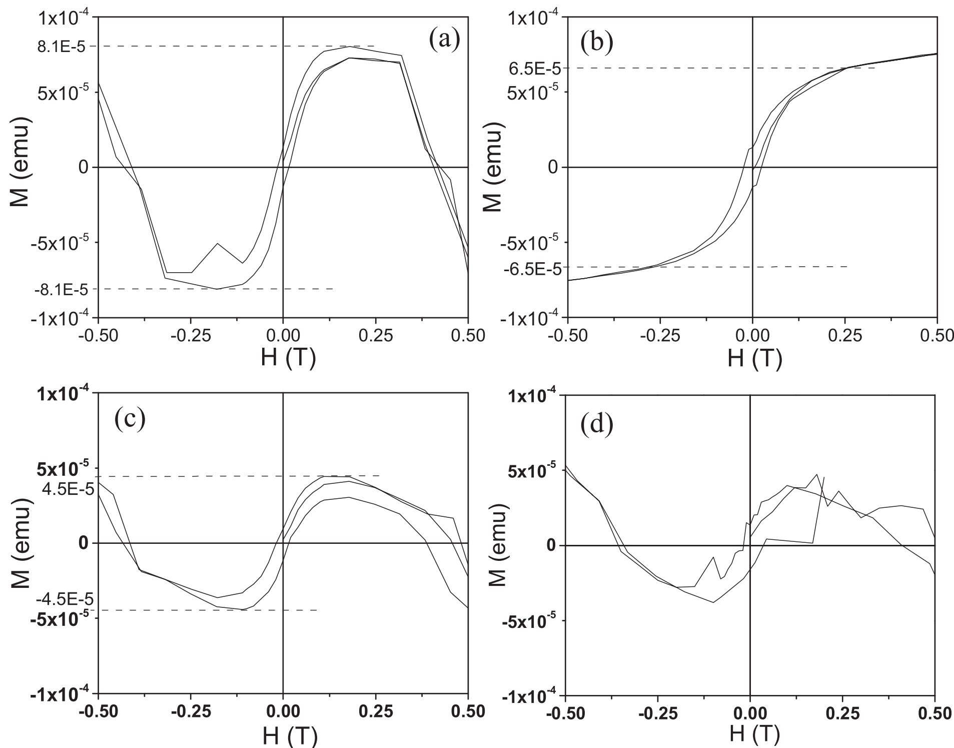

FIG. 9. M-H raw curves at 100 K of samples (a) 2, (b) 3, (c) 4, and (d) 5 showing ferromagnetic order that, in sample 3, overcomes the diamagnetic response of the substrate. It is also clear that the FM signal and the magnetization M decrease with the increasing atomic percentage of O as shown in the M-H curves of samples 4 and 5, (c) and (d), respectively.

ferromagnetism, as other authors have suggested. Ren *et al.* and Jeganathan *et al.*[44,45] recently reported ferromagnetism in gallium-deficient GaN nanoparticles and nanowires, respectively, in which both groups vary the Ga flux during the synthesis of the nanostructures and correlate the gallium deficiency, detected by EDS or XPS, to the generation of V_{Ga}. These measures were correlated with PL measurements that confirmed the presence of gallium vacancies due to its electronic transitions, similarly to the CL measurements present in this work, because the sensitivity of these techniques to detect the characteristic defect-related optical transition has been broadly demonstrated.[36] Figures 9(c) and 9(d) show the M-H curves of samples 4 and 5, respectively, revealing a gradual loss of the ferromagnetic signal, which is noticeable in the reduction of the magnetization range compared with samples S2 and S3 (blue dotted lines). It is difficult to assign a saturation point due to the poor crystallinity of sample S5, but a weak FM signal is still observed. The reduction in the FM signal is an effect of the incorporation of oxygen as an impurity into both samples (Table I), which lowers the crystalline quality of GaN as seen in Fig. 1 and the interaction or bonding of Mn with the elements on the GaN lattice that in turn participates in the generation of FM in GaN:Mn systems.

IV. CONCLUSIONS

Mn-doped GaN microstructures were synthesized by thermal evaporation of GaN and $MnCO_3$ powders onto $Ni_{0.8}Cr_{0.2}$/Si(100) in a horizontal furnace operated at low vacuum. Residual air inside the system was used as a source of oxygen during the synthesis of Mn and O co-doped GaN nanostructures. Mn and O impurities were incorporated into the nanostructures at different concentrations by varying the growth temperature. EDS, XRD, and XPS measurements confirmed that the obtained samples predominantly consisted of GaN. XRD results revealed that the nanostructures crystallinity of the nanostructures diminished with increasing oxygen concentrations. HRTEM images revealed that the incorporation of oxygen generates stacking fault defects. Sample CL spectra showed that Mn incorporation at a concentration of 8.9 at. % generates defect-related emissions of 2.45 and 2.9 attributed to gallium vacancies (V_{Ga}), in addition to an emission of 1.97 eV assigned to transitions between the $4T_1$-$6A_1$ states of the Mn^{2+} d orbitals. The magnetic response of the samples revealed a ferromagnetic signal that correlated with the Mn concentration and with the generation of V_{Ga} point defects.

SUPPLEMENTARY MATERIAL

See supplementary material for the secondary images of the samples on the areas where EDS measurements were acquired and their respective energy spectra with the detected elements.

ACKNOWLEDGMENTS

This work was supported by PAPIIT-UNAM and CONACYT (Project Nos. IN101917 and INFR-2011-1-163153). G.G. acknowledges the Ph.D. scholarship granted by CONACYT (Grant No. 227762, CVU 296835) and additional financing through the funding program for Ph.D. student from CONACYT-CICESE. R.E. acknowledges support by Project DGAPA IT100217 and A. Lopez and A. Pompa-Garcia for technical support. The technical support of A. Duran, E. Aparicio, F. Ruiz, V. Gómez, and D. Dominguez is greatly appreciated. M. I. Perez Montfort corrected the English version of the manuscript.

[1]S. Zhou, S. Wang, S. Liu, and H. Ding, Opt. Laser Technol. **54**, 321 (2013).
[2]A. Kumar, A. Hähnel, D. Kanjilal, and R. Singh, Appl. Phys. Lett. **101**, 153508 (2012).
[3]K. H. Baik, H. Kim, J. Kim, S. Jung, and S. Jang, Appl. Phys. Lett. **103**, 91107 (2013).
[4]Z. H. Zhang, S. T. Tan, Z. Kyaw, Y. Ji, W. Liu, Z. Ju, N. Hasanov, X. W. Sun, and H. V. Demir, Appl. Phys. Lett. **102**, 193508 (2013).
[5]T. T. Dietl, H. Ohno, F. Matsukura, J. Cibert, and D. Ferrand, Science **287**, 1019 (2000).
[6]J. I. Hwang, M. Kobayashi, G. S. Song, A. Fujimori, A. Tanaka, Z. S. Yang, H. J. Lin, D. J. Huang, C. T. Chen, H. C. Jeon, and T. W. Kang, Appl. Phys. Lett. **91**, 072507 (2007).
[7]D. S. Han, J. Park, K. W. Rhie, S. Kim, and J. Chang, Appl. Phys. Lett. **86**, 032506 (2005).
[8]D. Chen, Z. Ding, S. Yao, W. Hua, K. Wang, and T. Chen, Nucl. Instrum. Methods Phys. Res., Sect. B **266**, 2797 (2008).
[9]D. M. G. Leite, A. L. J. Pereira, W. A. Iwamoto, P. G. Pagliuso, P. N. Lisboa-Filho, and J. H. D. da Silva, Solid State Sci. **17**, 97 (2013).
[10]J. M. D. Coey, M. Venkatesan, and C. B. Fitzgerald, Nat. Mater. **4**, 173 (2005).
[11]M. Xiao, T. Yao, Z. A, P. Wei, D. Wang, and H. Song, Phys. Chem. Chem. Phys. **17**, 8692 (2015).
[12]Z. Min and S. J. Jie, Chin. Phys. B **23**, 017301 (2014).
[13]X.-W. Zhang, J. Li, K. Chang, S.-S. Li, and J.-B. Xia, J. Appl. Phys. **109**, 074313 (2011).
[14]M. H. F. Sluiter, Y. Kawazoe, P. Sharma, A. Inoue, A. R. Raju, and C. Rout, Phys. Rev. Lett. **94**, 187204 (2005).
[15]J. J. Liu, K. Wang, M. H. Yu, and W. L. Zhou, J. Appl. Phys. **102**, 024301 (2007).
[16]X. G. Xu, H. L. Yang, Y. Wu, D. L. Zhang, S. Z. Wu, J. Miao, Y. Jiang, X. B. Qin, X. Z. Cao, and B. Y. Wang, Appl. Phys. Lett. **97**, 232502 (2010).
[17]H. W. Peng, H. J. Xiang, S. H. Wei, S. S. Li, J. B. Xia, and J. B. Li, Phys. Rev. Lett. **102**, 017201 (2009).
[18]G. Guzmán and M. Herrera, Semicond. Sci. Technol. **29**, 025001 (2014).
[19]G. Guzmán, M. Herrera, R. Silva, G. C. Vásquez, and D. Maestre, Semicond. Sci. Technol. **31**, 055006 (2016).
[20]G. Guzmán-Navarro, M. Herrera-Zaldivar, J. Valenzuela-Benavides, and D. Maestre, J. Appl. Phys. **110**, 034315 (2011).
[21]J. Neugebauer and C. Van de Walle, Phys. Rev. B **50**, 8067 (1994).
[22]V. Thakur and S. M. Shivaprasad, Appl. Surf. Sci. **327**, 389 (2015).
[23]M. Kumar, A. Kumar, S. B. Thapa, S. Christiansen, and R. Singh, Mater. Sci. Eng., B **186**, 89 (2014).
[24]See https://srdata.nist.gov/xps/ for NIST (National Institute of Standards and Technology, Gaithersburg) X-ray Photoelectron Spectroscopy Database, Version 4.1 (2012).
[25]M. Meng, S. X. Wu, L. Z. Ren, W. Q. Zhou, Y. J. Wang, G. L. Wang, and S. W. Li, J. Appl. Phys. **116**, 173911 (2014).
[26]Y. Liu, L. Xu, X. Li, P. Hu, and S. Li, J. Appl. Phys. **107**, 103914 (2010).
[27]Z. Huang, W. Zhou, C. Ouyang, J. Wu, F. Zhang, J. Huang, Y. Gao, and J. Chu, Sci. Rep. **5**, 10899 (2015).
[28]J. I. Hwang, Y. Ishida, M. Kobayashi, H. Hirata, K. Takubo, T. Mizokawa, A. Fujimori, J. Okamoto, K. Mamiya, Y. Saito, Y. Muramatsu, H. Ott, A. Tanaka, T. Kondo, and H. Munekata, Phys. Rev. B **72**, 085216 (2005).
[29]X. Cui and J. Zhang, Opt. Mater. **46**, 299 (2015).
[30]P. Bogusławski and J. Bernholc, Phys. Rev. B **72**, 115208 (2005).
[31]G. I. Taylor, Proc. R. Soc. London, Ser. A **145**, 362–387 (1934).
[32]J. P. Hirth and J. Lothe, *Theory of Dislocations*, 2nd ed. (Krieger Publ. Co., 1992), ISBN: 0-89464-617-6.
[33]M. Herrera, A. Cremades, M. Stutzmann, and J. Piqueras, Superlattices Microstruct. **45**, 435 (2009).

[34]D. M. Hofmann, D. Kovalev, G. Stende, B. K. Meyer, A. Hoffmann, L. Eckey, R. Heitz, T. Detchprom, H. Amano, and I. Akasaki, Phys. Rev. B **52**, 16072 (1995).
[35]M. Herrera-Zaldívar, P. Fernández, and J. Piqueras, Semicond. Sci. Technol. **13**, 900 (1998).
[36]M. A. Reshchikova and H. Morkoç, J. Appl. Phys. **97**, 061301 (2005).
[37]N. Joshi, H. Medina, A. Cantarero, and O. Ambacher, J. Phys. Chem. Solids **64**, 1685 (2003).
[38]T. Graf, M. Gjukic, M. S. Brandt, and M. Stutzmann, Appl. Phys. Lett. **81**, 5159 (2002).
[39]S. J. Xu, G. Li, S. J. Chua, X. C. Wang, and W. Wang, Appl. Phys. Lett. **72**, 2451 (1998).
[40]M. A. Reshchikov, F. Shahedipour, R. Y. Korotkov, B. W. Wessels, and M. P. Ulmer, J. Appl. Phys. **87**, 3351 (2000).
[41]J. Elsner, R. Jones, M. I. Heggie, P. K. Sitch, M. Haugk, T. Frauenheim, S. Öberg, and P. R. Briddon, Phys. Rev. B **58**, 12571 (1998).
[42]M. Herrera-Zaldívar, P. Fernández, and J. Piqueras, J. Appl. Phys. **83**, 2796 (1998).
[43]H. Hori, S. Sonoda, T. Sasaki, Y. Yamamoto, S. Shimizu, K. Suga, and K. Kindo, Physica B **324**, 142 (2002).
[44]H. Ren, J. Jian, C. Chen, D. Pan, A. Ablat, Y. Sun, J. Li, and R. Wu, Appl. Phys. A **116**, 185 (2014).
[45]K. Jeganathan, V. Purushothaman, R. Debnath, and S. Arumugam, AIP Adv. **4**, 057116 (2014).